

The Interstitial Carbon–Dioxygen Center in Irradiated Silicon

Postidi, M., Kuganathan, N., Christopoulos, S., Chroneos, A., Angeletos, T., Sarlis, N. & Londis, C.

Published PDF deposited in Coventry University's Repository

Original citation:

Postidi, M, Kuganathan, N, Christopoulos, S, Chroneos, A, Angeletos, T, Sarlis, N & Londis, C 2020, 'The Interstitial Carbon–Dioxygen Center in Irradiated Silicon', Crystals, vol. 10, no. 11, 1005.

<https://dx.doi.org/10.3390/cryst10111005>

DOI 10.3390/cryst10111005

ESSN 2073-4352





Publisher: MDPI

This article is an open access article distributed under the terms and conditions of the Creative Commons Attribution (CC BY) license (<http://creativecommons.org/licenses/by/4.0/>).

Copyright © and Moral Rights are retained by the author(s) and/ or other copyright owners. A copy can be downloaded for personal non-commercial research or study, without prior permission or charge. This item cannot be reproduced or quoted extensively from without first obtaining permission in writing from the copyright holder(s). The content must not be changed in any way or sold commercially in any format or medium without the formal permission of the copyright holders.

Article

The Interstitial Carbon–Dioxygen Center in Irradiated Silicon

Marianna S. Potsidi ¹, Navaratnarajah Kuganathan ^{2,3} , Stavros-Richard G. Christopoulos ² , Alexander ChronEOS ^{2,3,*} , Theoharis Angeletos ¹, Nicholas V. Sarlis ¹  and Charalampos A. Londos ^{1,*}

¹ Department of Physics, Solid State Physics Section, National and Kapodistrian University of Athens, Panepistimiopolis Zografos, 15784 Athens, Greece; mpotsidi@ea.gr (M.S.P.); t_angeletos@hotmail.com (T.A.); nsarlis@phys.uoa.gr (N.V.S.)

² Faculty of Engineering, Environment and Computing, Coventry University, Prior Street, Coventry CV1 5FB, UK; ad0636@coventry.ac.uk (N.K.); ac0966@coventry.ac.uk (S.-R.G.C.)

³ Department of Materials, Imperial College London, London SW7 2AZ, UK

* Correspondence: alexander.chroneos@imperial.ac.uk (A.C.); hlontos@phys.uoa.gr (C.A.L.)

Received: 4 October 2020; Accepted: 29 October 2020; Published: 5 November 2020



Abstract: We investigated, experimentally as well as theoretically, defect structures in electron irradiated Czochralski-grown silicon (Cz-Si) containing carbon. Infrared spectroscopy (IR) studies observed a band at 1020 cm^{-1} arisen in the spectra around $300\text{ }^{\circ}\text{C}$. Its growth occurs concomitantly with the decay out of the well-known vacancy-oxygen (VO) defect, with a Local Vibrational Mode (LVM) at 830 cm^{-1} and carbon interstitial-oxygen interstitial (C_iO_i) defect with a LVM at 862 cm^{-1} , in silicon (Si). The main purpose of this work is to establish the origin of the 1020 cm^{-1} band. One potential candidate is the carbon interstitial-dioxygen (C_iO_{2i}) defect since it is expected to form upon annealing out of the C_iO_i pair. To this end, systematic density functional theory (DFT) calculations were used to predict the lowest energy structure of the (C_iO_{2i}) defect in Si. Thereafter, we employed the dipole–dipole interaction method to calculate the vibrational frequencies of the structure. We found that C_iO_{2i} defect has an LVM at $\sim 1006\text{ cm}^{-1}$, a value very close to our experimental one. The analysis and study of the results lead us to tentatively correlate the 1020 cm^{-1} band with the C_iO_{2i} defect.

Keywords: silicon; irradiation; IR spectroscopy; DFT calculations

1. Introduction

The properties and behavior of semiconductors are affected by point defects and impurities introduced in the lattice during crystal growth and material processing. Si mainly contains carbon (C) and oxygen (O), which are unintentionally introduced impurities during crystal growth [1,2]. Upon irradiation, numerous reactions occur, leading to the formation of a variety of carbon-related and oxygen-related defects. Among these, the carbon interstitial (C_i), carbon interstitial-oxygen interstitial (C_iO_i), carbon interstitial-carbon substitutional (C_iC_s), and the vacancy-oxygen (VO), which give rise to electrical and optical signals and have been studied both theoretically and experimentally using a range of techniques [1–10]. Notably, the C_iO_i , C_iC_s , and the VO are important recombination centers with adverse effects on the performance of Si-based devices [8–10]. Upon thermal annealing, these defects participate in many reactions leading to the production of various complexes. Therefore, it is necessary to know all the properties and behavior of these defects in order to improve the performance of the relative devices.

In the present study, we mainly investigate defects formed upon annealing out of the C_iO_i pair. The latter defect anneals out mainly by dissociation [1,11]. However, C_iO_i pairs participate in

reactions with other defects where a small percentage of the C_iO_i migrate as an entity [1]. It has been suggested [12] that in the course of this migration, C_iO_i reacts with the VO. Both centers anneal out around 300 °C, and when they encounter, they lead to the formation of the carbon substitutional-dioxygen (C_sO_{2i}) defect, with a Local Vibrational Mode (LVM) frequency at 1048 cm^{-1} . Alternatively, C_sO_{2i} could form according to the reaction [13], $C_i + VO_2 \rightarrow C_sO_{2i}$. Reasonably, upon C_iO_i annealing, other carbon-related complexes could also form. Such complex is the carbon interstitial-dioxygen (C_iO_{2i}) defect [14,15]. In our studies, besides the 1048 cm^{-1} band, we have seen another one at 1020 cm^{-1} to arise in the spectra around 300 °C. This band is probably connected with the formation of new second-generation defects formed upon the disappearance of the C_iO_i pair. A potential candidate for the origin of the 1020 cm^{-1} band is the C_iO_{2i} complex.

In a recent theoretical study [15], the relevant reactions and the migration paths of the interstitial carbon and interstitial oxygen impurities in Si were explored in detail. In particular, a model was presented regarding the formation and dissociation mechanisms of the C_iO_i and the C_iO_{2i} complexes. The suggested [15] reaction paths for the formation of the latter defect involves (i) a further accumulation of oxygen in C_iO_i ($C_iO_i + O_i \rightarrow C_iO_{2i}$) or (ii) a reaction between C_i and O_{2i} ($C_i + O_{2i} \rightarrow C_iO_{2i}$). Formation mechanism (i) can occur via oxygen migration with an energy barrier of 2.53 eV, or C_iO_i migration, with a barrier of 2.45 eV. However, the dissociation of C_iO_i through reaction $C_iO_i \rightarrow C_i + O_i$, has a barrier of 2.29 eV, providing the necessary conditions for formation reaction ii) to occur, ending up to a more stable C_iO_{2i} complex, at a barrier of 2.33 eV. Early photoluminescence (PL) studies reported thermal treatments at 350–450 °C, have correlated the decay of the C-line (789.5 meV) of the C_iO_i defect with the growth of the P-line (767 meV) attributed to the C_iO_{2i} defect [1,16]. Recent deep level transient spectroscopy (DLTS) studies have monitored the decay of the C_iO_i pair and the formation of the C_iO_{2i} structure via the observation of the corresponding electronic levels at $E_V + 0.36$ eV and $E_V + 0.39$ eV [17]. These conclusions are in agreement with previous PL and DLTS measurements referring to the investigation of the C_iO_{2i} defect [18,19]. It was suggested that the annealing of the C_iO_i occurs via dissociation into C_i and O_i , where a percentage of the released C_i atoms are trapped by oxygen dimers to form the C_iO_{2i} [17,18].

Defects that introduce electronic levels in the gap most possibly affect the functionality of devices by deteriorating in general their performance. It is, therefore, important to identify the origin of any defect signal appearing in the measurements. In this work, we have employed Infrared spectroscopy (IR) measurements coupled with density functional theory (DFT) and dipole–dipole interaction calculations to investigate the 1020 cm^{-1} band in irradiated Si. The whole analysis of the results has led us to correlate the 1020 cm^{-1} band with the C_iO_{2i} defect.

2. Materials and Methods

2.1. Experimental

We used Czochralski (Cz-Si) p-type (boron-doped) samples with a resistivity of $\rho \sim 10 \Omega \text{ cm}$. The initial oxygen and carbon concentrations were $[O_i] = 1.1 \times 10^{18}$ and $[C_s] = 1.6 \times 10^{17} \text{ cm}^{-3}$, respectively. The samples were irradiated with 2 MeV electrons with a fluence of $1 \times 10^{18} \text{ cm}^{-2}$ at about 80 °C, using the Dynamitron accelerator at JAERI (Takasaki, Japan). After irradiation, the samples were subjected to isochronal anneals at selective temperatures up to ~600 °C in open furnaces. Successive anneals with increased temperature in steps of $\Delta T \sim 10$ °C and duration $\Delta t = 20$ min were conducted. After each annealing step, IR spectra were recorded at room temperature (RT) by means of a Fourier Transform Infrared (FTIR) spectrometer with a resolution of 1 cm^{-1} . The two phonon background absorption was always subtracted from each spectrum by using a Float-zone sample of equal thickness with that of the Cz samples.

2.2. Theoretical

Here, we employed spin-polarized DFT calculations using the Vienna Ab initio Simulation Package (VASP) code [20,21]. Plane wave basis sets and projected augmented wave (PAW) [22] potentials were applied to solve the standard Kohn–Sham (KS) equations. The supercell consisted of 250 Si atomic sites. The generalized gradient approximation (GGA) by Perdew, Burke, and Ernzerhof (PBE) [23] was employed for the exchange–correlation effects. The plane wave basis set extended to a cut-off of 500 eV. The $2 \times 2 \times 2$ Monkhorst-Pack [24] k-point mesh yielded 8 irreducible k-points. Both positions of atoms and lattice parameters were relaxed simultaneously for the Geometry optimizations (constant pressure conditions) using a conjugate gradient algorithm [25]. Convergence criteria were: Force tolerance 0.001 eV/Å and stress tensor 0.002 GPa. The dispersion interactions were accounted for in the form introduced by Grimme et al. [26]. The present calculations were well converged, and the adequacy of the present methodology was discussed in previous work [27–31].

3. Results

3.1. IR Measurements

Figure 1 represents characteristic segments of the IR spectra of electron irradiated Si samples, recorded after irradiation, and at the temperature of 350 °C in the course of the isochronal anneals performed in this experiment. Well-known bands at 830 cm^{-1} (VO), at 862 cm^{-1} (C_iO_i), and a pair at 936, 1020 cm^{-1} ($\text{C}_i\text{O}_i(\text{Si}_i)$), were present in the samples immediately after irradiation [30]. After the 350 °C anneal, the first two bands of VO and C_iO_i diminished substantially, although the pair of bands of the $\text{C}_i\text{O}_i(\text{Si}_i)$ defect disappeared as expected since they were stable up to ~180 °C [32]. Additionally, a set of new bands emerged in the spectra, those at 888 cm^{-1} (VO_2), 1048 cm^{-1} (C_sO_{2i}) [12,13], and another band at 1020 cm^{-1} . The latter band grown in the spectra at ~300 °C in the course of annealing was different from the 1020 cm^{-1} of the $\text{C}_i\text{O}_i(\text{Si}_i)$ defect appearing in the spectra immediately after irradiation. Its study is the main focus of the present work.

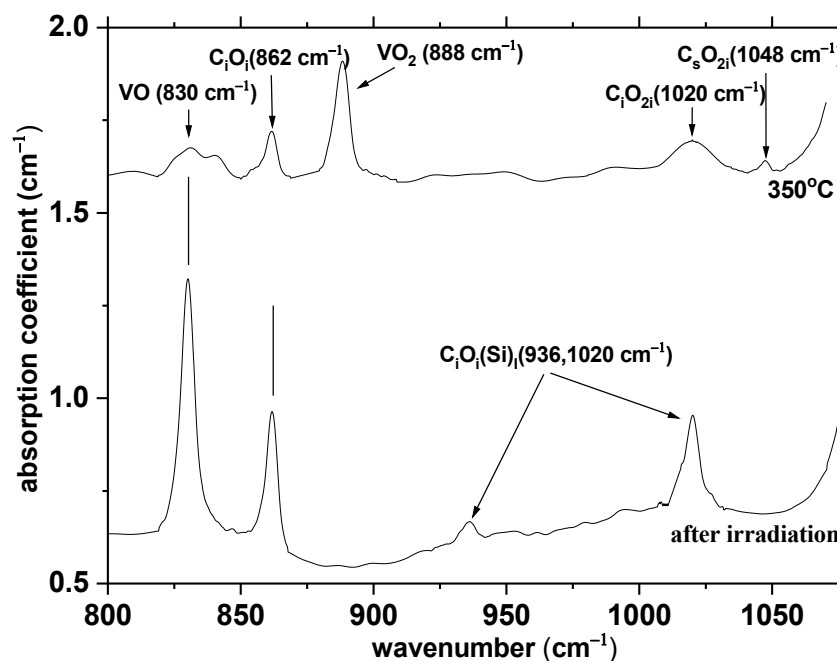


Figure 1. Segments of IR spectra of electron irradiated Si samples immediately after irradiation and at the characteristic T of 350 °C during the isochronal anneal sequence.

Figure 2 shows the thermal evolution of the VO, VO₂ as well as that of the C_iO_i and 1020 cm^{−1} bands. The latter band appeared in the spectra in the temperature range of 300 to 550 °C. Its evolution seemed to be connected with the decay of the C_iO_i defect and a potential candidate for its origin was the C_iO_{2i} structure. We have performed DFT calculations in conjunction with dipole–dipole interaction calculations to investigate the possible connection of the 1020 cm^{−1} band with the C_iO_{2i} structure.

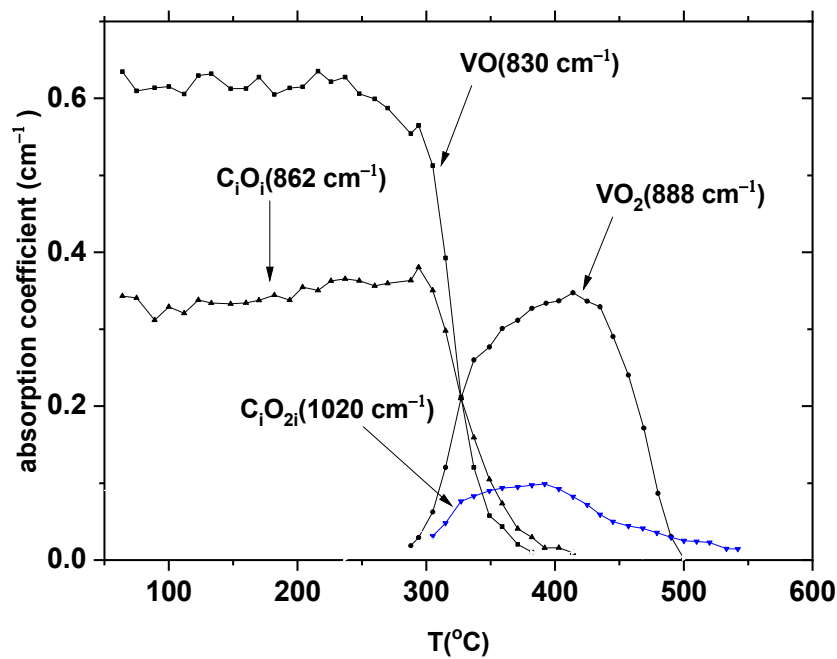


Figure 2. The thermal evolution of the 830 cm^{−1} (VO), 862 cm^{−1} (C_iO_i), 888 cm^{−1} (VO₂), and the 1020 cm^{−1} band.

3.2. DFT Results

Before proceeding, in order to be an agreement between the notation of DFT outcomes and that used in the dipole–dipole analysis, we will make a few remarks. When used, C refers to the C_i defect, O(1) refers to the O_i atom in the C_iO_i defect, and O(2) refers to the second O_i atom in the C_iO_{2i} defect. Thus, at some points, the C_iO_i defect is noted C–O(1).

The application of DFT calculations in the semiconductor materials is well established, and they can be used to provide information on the electronic properties and structure of point defects [33]. Considering defect clusters, their exact structure and geometry cannot be easily determined using experiments. This is an area where computational simulation can offer complementary information. To predict the prevalent structure, we considered all possible configurations (nearest neighbor, next nearest neighbor, and further apart) first for the C_iO_i and thereafter the C_iO_{2i} defect. The lowest energy C_iO_i defect is in excellent agreement with the structure previously reported [34–37] and references therein. Adding a further O_i leads to the formation of the C_iO_{2i} defect (refer to Figure 3). It should be stressed that the reported structure is the lowest energy one after systematically examining all possible configurations of the C_iO_{2i} defect in the Si lattice. This structure was thereafter adopted as the most possible one for our calculations.

For completeness, we also considered the density of states (DOS) plots and charge density plots (refer to Figure 4). There is a small gap state noted just below the Fermi level (refer to Figure 4a). This state belongs to the carbon interstitial, as confirmed by the atomic DOS of carbon (refer to Figure 4b). States belonging to the oxygen interstitial are mainly located in the deeper level (between 0 eV and 1 eV) (refer to Figure 4c,d). Charge density plots of oxygen di-interstitials are shown in Figure 4g,h. Decomposed charge density plot associated with carbon interstitial is delocalized over

Si atoms it bonded to. Decomposed charge density plots of oxygen interstitials delocalized over the square planar ring.

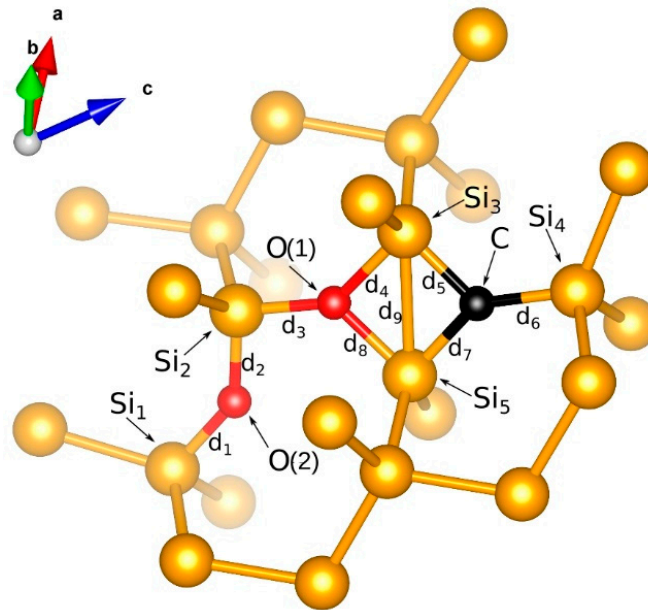


Figure 3. Schematic representation of the energetically favorable C_1O_{2i} defect. Bond distance values are: $d_1 = 1.665 \text{ \AA}$, $d_2 = 1.626 \text{ \AA}$, $d_3 = 1.711 \text{ \AA}$, $d_4 = 1.818 \text{ \AA}$, $d_5 = 1.765 \text{ \AA}$, $d_6 = 1.781 \text{ \AA}$, $d_7 = 1.782 \text{ \AA}$, $d_8 = 1.809 \text{ \AA}$, $d_9 = 2.571 \text{ \AA}$. Angle values are: $\text{Si}_1\text{-O(2)-Si}_2 = 140.85^\circ$, $\text{O(2)-Si}_2\text{-O(1)} = 99.04^\circ$, $\text{Si}_2\text{-O(1)-Si}_3 = 140.24^\circ$, $\text{Si}_2\text{-O(1)-Si}_5 = 129.45^\circ$, $\text{O(1)-Si}_3\text{-C} = 88.51^\circ$, $\text{O(1)-Si}_5\text{-C} = 88.25^\circ$, $\text{O(1)-Si}_3\text{-Si}_5 = 44.72^\circ$, $\text{O(1)-Si}_5\text{-Si}_3 = 44.98^\circ$, $\text{Si}_5\text{-Si}_3\text{-C} = 43.79^\circ$, $\text{Si}_3\text{-Si}_5\text{-C} = 43.27^\circ$, $\text{Si}_3\text{-C-Si}_4 = 125.69^\circ$, $\text{Si}_5\text{-C-Si}_4 = 141.37^\circ$.

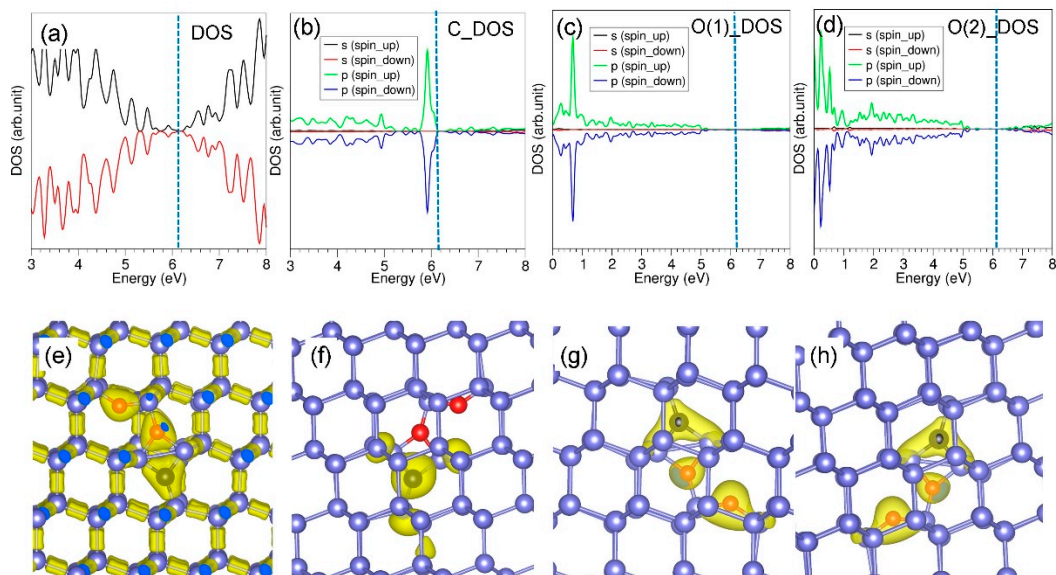


Figure 4. (a) Total DOS plot, (b) atomic DOS plot of carbon interstitial (C), (c) atomic DOS plot of the first oxygen interstitial (O(1)), (d) atomic DOS plot of the second oxygen interstitial (O(2)), (e) total charge density plot; decomposed charge density plots associated with (f) C, (g) O(1), and (h) O(2). Black circle refers to a carbon atom, and red circles refer to oxygen atoms.

3.3. LVM Estimations via the Dipole–Dipole Interaction Method

Figure 5 is a simplified structure model configuration of the C_iO_{2i} defect derived by DFT calculations. In essence, Figure 5 displays part of the lattice of Figure 3 containing the C and O(1) atoms settled in the (110) plane and the second oxygen interstitial atom, O(2). The C–O(1) direction forms an approximately 20° deeping angle with the $[\bar{1}10]$ direction (the Si_4 – Si_5 direction). Both C–O(1) and O(2) are IR active with reported [5] apparent charges and can be considered as two oscillating interacting dipoles.

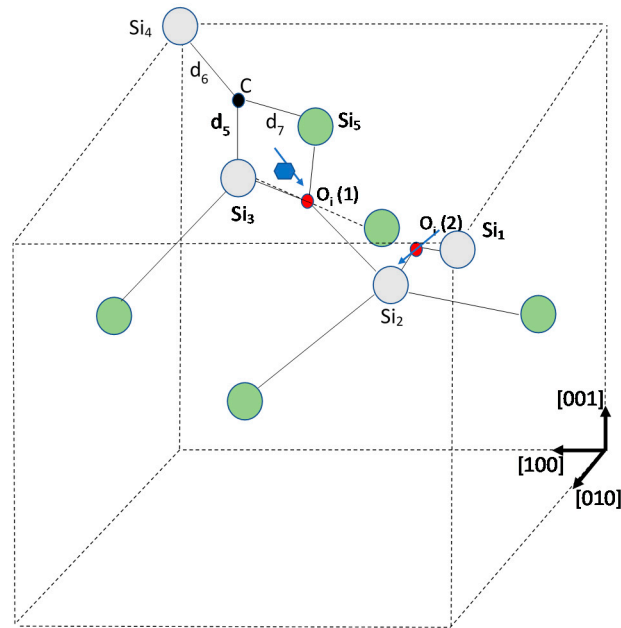


Figure 5. The C_iO_{2i} configuration. The blue hexagon corresponds to the reduced mass μ , of the C–O(1) dipole. Blue arrows indicate the oscillation directions of the C–O(1) and the O(2) dipoles.

Regarding the C–O(1) dipole, C and O(1) atoms are taken as one particle with mass corresponding to the reduced mass of oxygen and carbon atom μ , located at the center of mass, at distance d from O(1) atom. The reduced mass μ is derived from the relation

$$\mu = \frac{m_O m_C}{m_O + m_C} \quad (1)$$

while the distance d from the relation

$$d = \frac{m_C}{m_O + m_C} d_{C-O(1)} \quad (2)$$

where $m_O = 16 \text{ amu}$ and $m_C = 12 \text{ amu}$ are the masses of the oxygen and carbon atom, respectively and $d_{C-O(1)}$ is the distance between the C and O(1) atoms. The calculated values for μ and d , are $\mu = 11.38 \times 10^{-27} \text{ kg}$ and $d = 1.07 \text{ \AA}$, respectively.

The effective charge of C–O(1) is concentrated on the C–O(1) reduced mass and is equal to [5] $Z_{C-O(1)} = 2.4 |e|$, where $|e|$ is the electron charge. The effective charge concentrated on the O(2) atom is equal to [5] $Z_{O(2)} = 4.1 |e|$, where $|e|$ is the electron charge.

To estimate the LVM frequencies of the C_iO_{2i} defect, we applied a previously used procedure [38,39] based on the interaction of the C–O(1) and O(2) dipoles. The force constant of the perturbed oscillating C–O(1) entity is $K_{C-O(1)}$ and is given by the relation

$$K_{C-O(1)} = \mu \cdot (\omega_{C-O(1)})^2 \quad (3)$$

where $\omega_{\text{C-O}(1)}$ are the LVM frequencies of the C–O(1) defect. Similarly, the force constant of the oscillating O(2) atom, $K_{\text{O}(2)}$, is given by the relation

$$K_{\text{O}(2)} = m_{\text{O}} \cdot (\omega_{\text{O}(2)})^2 \quad (4)$$

and corresponds to the $\omega_{\text{O}(2)} = 1107 \text{ cm}^{-1}$ LVM frequency of the oxygen interstitial atom [2]. In this analysis, we use the values of $K_{\text{C-O}(1)}$ corresponding to the strongest experimentally detected LVM line at 862 cm^{-1} and the reported line [1,40] at 1116 cm^{-1} , both attributed to carbon-related modes.

We adopt the C–O(1) direction for the oscillation of the C–O(1) dipole and the $[1\bar{1}\bar{1}]$ for the oscillation [41] of the O(2) dipole. With the help of Figure 5, the expressions of the dipole moments $p_{\text{C-O}(1)}$ and $p_{\text{O}(2)}$ become

$$\begin{aligned} p_{\text{C-O}(1)} &= Z_{\text{C-O}(1)} q_1 \hat{q}_1 \\ p_{\text{O}(2)} &= Z_{\text{O}(2)} q_2 \hat{q}_2 \end{aligned} \quad (5)$$

where \hat{q}_1 , \hat{q}_2 are the unit vectors along the C–O(1) and $[1\bar{1}\bar{1}]$ directions, respectively. The potential energy of the interacting dipole moments is given by [42]

$$U_{\text{int}} = \frac{p_{\text{C-O}(1)} \cdot p_{\text{O}(2)} - 3(\hat{n} \cdot p_{\text{C-O}(1)})(\hat{n} \cdot p_{\text{O}(2)})}{d_{\mu\text{-O}(2)}^3} \quad (6)$$

where \hat{n} is the unit vector along the direction that connects the two dipoles and $d_{\mu\text{-O}(2)} = 3.36 \text{ \AA}$ is the distance between them. The motion of the two dipoles is described by the effective Hamiltonian

$$H = \frac{1}{2} \mu \dot{q}_1^2 + \frac{1}{2} m_{\text{O}} \dot{q}_2^2 + \frac{1}{2} K_{\text{C-O}(1)} q_1^2 + \frac{1}{2} K_{\text{O}(2)} q_2^2 + \lambda q_1 q_2 \quad (7)$$

By comparing Equations (6) and (7), we obtain the q-independent part λ , to be equal to $\lambda = 138 \text{ J/m}^2$. The Hamiltonian of Equation (7) has two normal modes with frequencies

$$\omega_{\text{C}_i\text{O}_{2i}} = \sqrt{\frac{1}{2} \left[\omega_{\text{C-O}(1)}^2 + \omega_{\text{O}(2)}^2 \pm \sqrt{(\omega_{\text{C-O}(1)} - \omega_{\text{O}(2)})^2 + \frac{4\lambda^2}{\mu \cdot m_{\text{O}}}} \right]} \quad (8)$$

where “+” preceding the inner square root corresponds to the antisymmetric normal mode and “−” to the symmetric one. For $\omega_{\text{C-O}(1)} = 862 \text{ cm}^{-1}$ and $\omega_{\text{O}(2)} = 1107 \text{ cm}^{-1}$ we find $\omega_{1, \text{C}_i\text{O}_{2i}}^{(\text{ant})} = 1098 \text{ cm}^{-1}$ and $\omega_{1, \text{C}_i\text{O}_{2i}}^{(\text{sym})} = 872 \text{ cm}^{-1}$. For $\omega_{\text{C-O}(1)} = 1116 \text{ cm}^{-1}$ and $\omega_{\text{O}(2)} = 1107 \text{ cm}^{-1}$ we find $\omega_{2, \text{C}_i\text{O}_{2i}}^{(\text{ant})} = 1205 \text{ cm}^{-1}$ and $\omega_{2, \text{C}_i\text{O}_{2i}}^{(\text{sym})} = 1006 \text{ cm}^{-1}$. Among them, we consider the band at 1006 cm^{-1} as the most possible candidate to be related to our experimental findings, as discussed below.

4. Discussion

The calculated frequency at 1006 cm^{-1} standing for the symmetric mode of the C_iO_{2i} related to the 1116 cm^{-1} carbon-related mode of the C–O(1) defect lies very close to the experimental line at 1020 cm^{-1} , supporting the attribution of this line to the C_iO_{2i} defect. Since the calculated dot product of the dipole moment vectors is positive, one would expect the symmetric modes at 872 and 1006 cm^{-1} to give stronger IR signals than the antisymmetric ones, at 1098 and 1205 cm^{-1} . In our spectra, only the symmetric mode at 1006 cm^{-1} is detectable. The other band at 872 cm^{-1} is not detected in our experiment. This is possibly because its weak signal is masked by the stronger signal of the VO_2 defect (Figure 1) in the same region. It is worth noting that if both dipoles oscillated along the direction connecting them, the theoretical outcome through the dipole–dipole interaction process would have provided a better fit (1021 cm^{-1}) to the experimental value at 1020 cm^{-1} .

The present calculations provide support for the notion that the 1020 cm^{-1} line can originate from the C_iO_{2i} defect. Regarding this correlation, it deserves noting that early IR studies of the evolution of carbon and its loss from solution, upon thermal treatments of Cz-Si at $450\text{ }^\circ\text{C}$, have revealed the formation of a band at 1026 cm^{-1} attributed to a carbon-oxygen dimer complex [43–45].

An important point: In our studies of electron irradiated silicon, the 1020 cm^{-1} band is formed around $300\text{ }^\circ\text{C}$ upon the decay of the 862 cm^{-1} band of the C_iO_i pair. However, in proton-irradiated thermally treated Si, the formation of the C_iO_{2i} occurs at temperatures above $400\text{ }^\circ\text{C}$ according to the reaction $\text{C}_i + \text{O}_{2i} \rightarrow \text{C}_i\text{O}_{2i}$ [17–19]. The suggested mechanism in the latter reports involves the dissociation of the C_iO_i and the capture of the liberated carbon interstitials by oxygen dimers. Profoundly, at these temperatures the availability of oxygen dimers plays an important role in the validity of the above reaction. In our case of electron irradiated silicon, C_iO_{2i} emerges in the spectra around $300\text{ }^\circ\text{C}$. However, the concentration of dimers at $\sim 300\text{ }^\circ\text{C}$ is practically negligible [2], and the reaction $\text{C}_i + \text{O}_{2i} \rightarrow \text{C}_i\text{O}_{2i}$ could not account for the formation of the C_iO_{2i} . Other reaction channels should govern the formation of the C_iO_{2i} in our case. One suggested reaction is the following: It is known that C_iO_i anneals out mainly by dissociation ($\text{C}_i\text{O}_i \rightarrow \text{C}_i + \text{O}_i$), but a small percentage of them could migrate in the lattice as an entity [1,15], being trapped by O_i atoms. This process leads to the formation of C_iO_{2i} structure ($\text{O}_i + \text{C}_i\text{O}_i \rightarrow \text{C}_i\text{O}_{2i}$). Additionally, another reaction mechanism could be envisaged. It is known that among the reactions that VO pair participates upon annealing, the main two are the following [7]: $\text{VO} + \text{O}_i \rightarrow \text{VO}_2$ and $\text{VO} + \text{Si}_i \rightarrow \text{O}_i$. In the latter reaction, sources of the participating self-interstitials are self-interstitial clusters formed in the course of the heavy irradiation of the Cz-Si [2]. In addition, O_i could be additionally provided [7] by the dissociation of VO. Since VO anneals out in parallel with C_iO_i , the following scheme is suggested. The liberated O_i atoms, in the course of VO dissociation or/and its destruction by self-interstitials, trap C_iO_i pairs leading to C_iO_{2i} complexes ($\text{VO} + \text{Si}_i \rightarrow \text{O}_i$, $\text{VO} \rightarrow \text{V} + \text{O}_i$, and then $\text{O}_i + \text{C}_i\text{O}_i \rightarrow \text{C}_i\text{O}_{2i}$). Apparently, the above two suggested reaction channels for the formation of the C_iO_{2i} defect may occur in parallel. Such reactions could account for the formation of the C_iO_{2i} in irradiated Si and explain its appearance at lower temperatures than those in thermally treated Si.

Regarding the differences in the formation temperature of the C_iO_{2i} defect between our electron irradiated samples and proton irradiated samples [17–19], the following should be noted: Proton irradiation generates higher order of damage than electron irradiation. This might result in more stable defects, which may need a higher temperature to anneal out. Additionally, the detected signal in our IR studies could refer to different states of the same defect reported in previous photoluminescence (PL) and DLTS measurements [17–19]. Further clarification of this issue requires future work.

Radiation defects in semiconductors attract a lot of interest, especially for technological purposes. Their presence in the Si lattice, in the course of material processing for special applications as for instance, radiation detectors, affect the device operation. Apparently, any information for such defects may improve the device functionality since it provides opportunities for their control. The present study is an attempt to determine the origin of an IR signal at 1020 cm^{-1} . We have connected it with a second-order generation carbon-oxygen related defect, that is the C_iO_{2i} complex. In future work we shall use higher irradiation fluencies to study the annealing of the C_iO_{2i} defect and the formation of larger complexes in this family of defects as the C_iO_{3i} structure, recently predicted theoretically [15].

5. Conclusions

The annealing of defects in irradiated Cz-Si revealed a new IR band at 1020 cm^{-1} emerging in the spectra around $300\text{ }^\circ\text{C}$ upon the decay of the 862 cm^{-1} band of the C_iO_i defect. PL and DLTS data have previously correlated certain signals with the formation of a C_iO_{2i} defect grown in the spectra upon the decay of the C_iO_i defect. In the present study, we employed systematic DFT calculations to gain an understanding of the lowest energy structure of the C_iO_{2i} defect. Thereafter, the dipole–dipole interaction calculations have estimated an LVM frequency at 1006 cm^{-1} related to

this center. This value lies very close to the experimental one at 1020 cm^{-1} . We have assigned the latter band to the C_iO_{2i} defect.

Author Contributions: Formal analysis, T.A., N.V.S. and C.A.L.; methodology, M.S.P., N.K., S.-R.G.C., and C.A.L.; supervision, A.C.; writing—original draft, M.S.P., N.K., S.-R.G.C., and C.A.L.; writing—review and editing, A.C. and N.V.S. All authors have read and agreed to the published version of the manuscript.

Funding: This research received no external funding.

Acknowledgments: T. Angeletos is grateful to the A. S. Onassis Foundation for financial support through his Ph.D. scholarship (Grant No. G ZL 001-1/2015-2016).

Conflicts of Interest: The authors declare no conflict of interest.

References

1. Davies, G.; Newman, R.C. Carbon in Monocrystalline Silicon. In *Handbook on Semiconductors*; Completely Revised ed.; Moss, T.S., Mahajan, S., Eds.; Elsevier Science, B.V.: Amsterdam, The Netherlands, 1994; Volume 3, pp. 1557–1635.
2. Newman, R.C.; Jones, R. Diffusion of Oxygen in Silicon. In *Semiconductors and Semimetals: Oxygen in Silicon*; Shimura, F., Ed.; Academic Press: Orlando, FL, USA, 1994; Volume 42, pp. 289–352.
3. Londos, C.A. Annealing Studies of Defects Pertinent to Radiation Damage in Silicon. *Phys. Stat. Sol.* **1987**, *102*, 639–644. [[CrossRef](#)]
4. Ferenczi, G.; Londos, C.A.; Pavelka, T.; Somogyi, M. Correlation of the concentration of the carbon-associated radiation damage levels with the total carbon concentration in silicon. *J. Appl. Phys.* **1988**, *63*, 183–189. [[CrossRef](#)]
5. Chappell, S.P.; Claybourn, M.; Newman, R.C.; Barraclough, K.G. The production of $\text{C}_i\text{-O}_i$ complexes during irradiation of Czochralski silicon at 130 K. *Semicond. Sci. Technol.* **1988**, *3*, 1047–1051. [[CrossRef](#)]
6. Watkins, G.D.; Corbett, J.W. Defects in Irradiated Silicon. I. Electron Spin Resonance of the Si-A Center. *Phys. Rev.* **1961**, *121*, 1001–1014. [[CrossRef](#)]
7. Londos, C.A.; Andrianakis, A.; Sgourou, E.N.; Emtsev, V.V.; Ohyama, H. IR studies of the impact of Ge doping on the successive conversion of VO_n defects in Czochralski-Si containing carbon. *J. Appl. Phys.* **2011**, *109*, 1–8. [[CrossRef](#)]
8. Tsuchiya, D.; Sueoka, K.; Yamamoto, H. Density Functional Theory Study on Defect Behavior Related to the Bulk Lifetime of Silicon Crystals for Power device Application. *Phys. Status Solidi A* **2019**, *216*, 1–17. [[CrossRef](#)]
9. Brotherton, S.D.; Bradley, P.J. Defect production and lifetime control in electron and γ -irradiated silicon. *Appl. Phys.* **1982**, *53*, 5720–5732. [[CrossRef](#)]
10. Siemienieć, M.; Niedernostheide, F.-J.; Schlze, H.-J.; Sudkamp, W.; Kellner-Werdehausen, U.; Lutz, J. Irradiation-Induced Deep Levels in Silicon for Power Device Tailoring. *J. Electrochem. Soc.* **2006**, *153*, G108–G118. [[CrossRef](#)]
11. Svensson, B.G.; Lindström, J.L. Annealing Studies of the 862 cm^{-1} Infrared Band in Silicon. *Phys. Stat. Sol.* **1987**, *95*, 537–542. [[CrossRef](#)]
12. Inoue, N.; Ohyama, H.; Goto, Y.; Sugiyama, T. Quantitative analysis of complexes in electron irradiated CZ silicon. *Physica B* **2007**, *401*, 477–482. [[CrossRef](#)]
13. Murin, L.I.; Markevich, V.P.; Lindstrom, J.L.; Kleverman, M.; Hermansson, J.; Hallberg, T.; Svensson, B.G. Carbon-Oxygen-Related Complexes in Irradiated and Heat-Treated Silicon: IR Absorption Studies. *Solid State Phenom.* **2002**, *82*, 57–62. [[CrossRef](#)]
14. Ewels, C.P.; Jones, R.; Oberg, S. Oxygen-Carbon, Oxygen-Nitrogen and Oxygen Dimer Defects in Silicon. In *Early Stages of Oxygen Precipitation in Silicon*; Jones, R., Ed.; Kluwer Academic Publishers: London, UK, 1996; Volume 17, pp. 141–162.
15. Ayed, H.M.; Monakhov, E.V.; Coutinho, J. Formation and dissociation reactions of complexes involving interstitial carbon and oxygen defects in silicon. *Phys. Rev. Mater.* **2020**, *4*, 064601. [[CrossRef](#)]
16. Kürner, W.; Sauer, R.; Dornen, A.; Thonke, K. Structure of the 0.767-eV oxygen-carbon luminescence defect in 450°C thermally annealed Czochralski-grown silicon. *Phys. Rev. B* **1989**, *39*, 13327–13337. [[CrossRef](#)] [[PubMed](#)]

17. Ayedh, H.M.; Grigorev, A.A.; Galeckas, A.; Svensson, B.G.; Monakhov, E.V. Annealing Kinetics of the Interstitial Carbon-Dioxygen Complex in Silicon. *Phys. Status Solidi A* **2019**, *216*, 1–5. [\[CrossRef\]](#)
18. Ganagona, N.; Raeissi, B.; Vines, L.; Monakhov, E.V.; Svensson, B.G. Defects in p-type Cz-silicon irradiated at elevated temperatures. *Phys. Status Solidi C* **2012**, *9*, 2009–2012. [\[CrossRef\]](#)
19. Raeissi, B.; Ganagona, N.; Galeckas, A.; Monakhov, E.V.; Svensson, B.G. PL and DLTS analysis of carbon-related centers in irradiated p-type Cz-Si. *Solid State Phenom.* **2014**, *205*, 224–227. [\[CrossRef\]](#)
20. Kresse, G.; Furthmüller, J. Efficient iterative schemes for ab initio-energy calculations using a plane-wave basis set. *Phys. Rev. B* **1996**, *54*, 11169–11186. [\[CrossRef\]](#)
21. Kresse, G.; Joubert, D. From ultrasoft pseudopotentials to the projector augmented-wave method. *Phys. Rev. B* **1999**, *59*, 1758–1775. [\[CrossRef\]](#)
22. Blöchl, P.E. Projector augmented-wave method. *Phys. Rev. B* **1994**, *50*, 17953–17979. [\[CrossRef\]](#)
23. Perdew, J.P.; Burke, K.; Ernzerhof, M. Generalized Gradient Approximation Made Simple. *Phys. Rev. Lett.* **1996**, *77*, 3865–3868. [\[CrossRef\]](#)
24. Monkhorst, H.J.; Pack, J.D. Special points for Brillouin-zone integration. *Phys. Rev. B* **1976**, *13*, 5188–5192. [\[CrossRef\]](#)
25. Press, W.H.; Teukolsky, S.A.; Vetterling, W.T.; Flannery, B.P. *Numerical Recipes in C: The Art of Scientific Computing*, 2nd ed.; Cambridge University Press: Cambridge, UK, 1992.
26. Grimme, S.; Antony, J.; Ehrlich, S.; Krieg, H. A consistent and accurate ab initio parametrization of density functional dispersion correction (DFT-D) for the 94 elements H–Pu. *J. Chem. Phys.* **2010**, *132*, 1–19. [\[CrossRef\]](#)
27. Chroneos, A.; Bracht, H.; Grimes, R.W.; Uberuaga, B.P. Phosphorus clustering in germanium-rich silicon germanium. *Mater. Sci. Eng. B* **2008**, *154*, 72–75. [\[CrossRef\]](#)
28. Chroneos, A.; Jiang, C.; Grimes, R.W.; Schwingenschlögl, U.; Bracht, H. E centers in ternary $\text{Si}_{1-x-y}\text{Ge}_x\text{Sn}_y$ random alloys. *Appl. Phys. Lett.* **2009**, *95*, 1–3. [\[CrossRef\]](#)
29. Chroneos, A.; Londos, C.A. Interaction of A-centers with isovalent impurities in silicon. *J. Appl. Phys.* **2010**, *107*, 1–4. [\[CrossRef\]](#)
30. Sgourou, E.N.; Timerkaeva, D.; Londos, C.A.; Aliprantis, D.; Chroneos, A.; Caliste, D.; Pochet, P. Impact of isovalent doping on the trapping of vacancy and interstitial defects in silicon. *J. Appl. Phys.* **2013**, *113*, 113506. [\[CrossRef\]](#)
31. Wang, H.; Chroneos, A.; Londos, C.A.; Sgourou, E.N.; Schwingenschlögl, U. A-centers in silicon with hybrid density functional theory. *Appl. Phys. Lett.* **2013**, *103*, 052101. [\[CrossRef\]](#)
32. Londos, C.A.; Sgourou, E.N.; Chroneos, A.; Emtsev, V.V. Carbon, oxygen and intrinsic defect interactions in germanium-doped silicon. *Semicond. Sci. Technol.* **2011**, *26*, 1–6. [\[CrossRef\]](#)
33. Chroneos, A.; Sgourou, E.N.; Londos, C.A.; Schwingenschlögl, U. Oxygen defect processes in silicon and silicon germanium. *Appl. Phys. Rev.* **2015**, *2*, 021306. [\[CrossRef\]](#)
34. Khirunenko, L.I.; Sosnin, M.G.; Pomozov, Y.V.; Murin, L.I.; Markevich, V.P.; Peaker, A.R.; Almeida, L.M.; Coutinho, J.; Torres, V.J.B. Formation of interstitial carbon-interstitial oxygen complexes in silicon: Local vibrational mode spectroscopy and density functional theory. *Phys. Rev. B* **2008**, *78*, 155203. [\[CrossRef\]](#)
35. Coutinho, J.; Jones, R.; Briddon, P.R.; Öberg, S.; Murin, L.I.; Markevich, V.P.; Lindström, J.L. Interstitial carbon-oxygen center and hydrogen related shallow thermal donors in Si. *Phys. Rev. B* **2001**, *65*, 014109. [\[CrossRef\]](#)
36. Backlund, D.J.; Estreicher, S.K. C_4 defect and its precursors in Si: First principles theory. *Phys. Rev. B* **2008**, *77*, 1–8. [\[CrossRef\]](#)
37. Wang, H.; Chroneos, A.; Londos, C.A.; Sgourou, E.N.; Schwingenschlögl, U. Carbon related defects in irradiated silicon revisited. *Sci. Rep.* **2014**, *4*, 1–9. [\[CrossRef\]](#) [\[PubMed\]](#)
38. Sarlis, N.V.; Londos, C.A.; Fytros, L.G. Origin of infrared bands in neutron-irradiated silicon. *J. Appl. Phys.* **1997**, *81*, 1645–1650. [\[CrossRef\]](#)
39. Potsidi, M.S.; Londos, C.A. The $\text{C}_i\text{C}_s(\text{Si}_i)$ defect in silicon: An infrared spectroscopy study. *J. Appl. Phys.* **2006**, *100*, 1–4. [\[CrossRef\]](#)
40. Davies, G.; Hayama, S.; Hao, S.; Bech Nielsen, B.; Coutinho, J.; Sanati, M.; Estreicher, S.K.; Itoh, K.M. Host isotope effects on midinfrared optical transitions in silicon. *Phys. Rev. B* **2005**, *71*, 1–7. [\[CrossRef\]](#)
41. Mc Cluskey, M.D. Local vibrational modes of impurities in semiconductors. *J. Appl. Phys.* **2000**, *87*, 3593–3617. [\[CrossRef\]](#)

42. Jackson, J. *Classical Electrodynamics*, 2nd ed.; Wiley: New York, NY, USA, 1975; p. 136.
43. Bean, A.R.; Newman, R.C. The effect of carbon on thermal donor formation in heat treated pulled silicon crystals. *J. Phys. Chem. Solids* **1972**, *33*, 251–268. [[CrossRef](#)]
44. Newman, R.C.; Oates, A.S.; Livingston, F.M. Self-interstitials and thermal donor formation in silicon: New measurements and a model for the defects. *J. Phys. C Solid State Phys.* **1983**, *16*, L667–L674. [[CrossRef](#)]
45. Lindström, J.L.; Werman, H.; Oehrlein, G.S. Thermal donors and carbon-Oxygen defects in silicon. *Phys. Status Solid A* **1987**, *99*, 581–591. [[CrossRef](#)]

Publisher’s Note: MDPI stays neutral with regard to jurisdictional claims in published maps and institutional affiliations.



© 2020 by the authors. Licensee MDPI, Basel, Switzerland. This article is an open access article distributed under the terms and conditions of the Creative Commons Attribution (CC BY) license (<http://creativecommons.org/licenses/by/4.0/>).